



AFRL-RX-WP-TR-2016-0013

**METALLIC AND CERAMIC MATERIALS RESEARCH
Task Order 0005: Metallic, Materials, Methods, Characterization
and Testing Research**

**Sang-Lan Kim, David S. Lee, Triplicane A. Parthasarathy, Satish I. Rao, Oleg N. Senkov,
James M. Scott, and Vikas Sinha
UES Inc.**

**OCTOBER 2015
Final Report**

Distribution Statement A. Approved for public release; distribution unlimited.

See additional restrictions described on inside pages

STINFO COPY

**AIR FORCE RESEARCH LABORATORY
MATERIALS AND MANUFACTURING DIRECTORATE
WRIGHT-PATTERSON AIR FORCE BASE, OH 45433-7750
AIR FORCE MATERIEL COMMAND
UNITED STATES AIR FORCE**

NOTICE AND SIGNATURE PAGE

Using Government drawings, specifications, or other data included in this document for any purpose other than Government procurement does not in any way obligate the U.S. Government. The fact that the Government formulated or supplied the drawings, specifications, or other data does not license the holder or any other person or corporation; or convey any rights or permission to manufacture, use, or sell any patented invention that may relate to them.

This report was cleared for public release by the USAF 88th Air Base Wing (88 ABW) Public Affairs Office (PAO) and is available to the general public, including foreign nationals.

Copies may be obtained from the Defense Technical Information Center (DTIC) (<http://www.dtic.mil>).

AFRL-RX-WP-TR-2016-0013 HAS BEEN REVIEWED AND IS APPROVED FOR PUBLICATION IN ACCORDANCE WITH ASSIGNED DISTRIBUTION STATEMENT.

//Signature//

PATRICK CARLIN, Project Engineer
Composite Materials and Processing Section
Composite Branch
Structural Materials Division

//Signature//

DANIEL EVANS, Chief
Metals Branch
Structural Materials Division

//Signature//

ROBERT T. MARSHALL, Deputy Chief
Structural Materials Division
Materials and Manufacturing Directorate

This report is published in the interest of scientific and technical information exchange, and its publication does not constitute the Government's approval or disapproval of its ideas or findings.

REPORT DOCUMENTATION PAGE

Form Approved
OMB No. 0704-0188

The public reporting burden for this collection of information is estimated to average 1 hour per response, including the time for reviewing instructions, searching existing data sources, searching existing data sources, gathering and maintaining the data needed, and completing and reviewing the collection of information. Send comments regarding this burden estimate or any other aspect of this collection of information, including suggestions for reducing this burden, to Department of Defense, Washington Headquarters Services, Directorate for Information Operations and Reports (0704-0188), 1215 Jefferson Davis Highway, Suite 1204, Arlington, VA 22202-4302. Respondents should be aware that notwithstanding any other provision of law, no person shall be subject to any penalty for failing to comply with a collection of information if it does not display a currently valid OMB control number. **PLEASE DO NOT RETURN YOUR FORM TO THE ABOVE ADDRESS.**

1. REPORT DATE (DD-MM-YY) October 2015			2. REPORT TYPE Final		3. DATES COVERED (From - To) 22 September 2014 – 21 September 2015	
4. TITLE AND SUBTITLE METALLIC AND CERAMIC MATERIALS RESEARCH Task Order 0005: Metallic, Materials, Methods, Characterization and Testing Research					5a. CONTRACT NUMBER FA8650-10-D-5226-0005	
					5b. GRANT NUMBER	
					5c. PROGRAM ELEMENT NUMBER 62102F	
6. AUTHOR(S) Sang-Lan Kim, David S. Lee, Triplicane A. Parthasarathy, Satish I. Rao, Oleg N. Senkov, James M. Scott, and Vikas Sinha					5d. PROJECT NUMBER 4347	
					5e. TASK NUMBER	
					5f. WORK UNIT NUMBER X0UP	
7. PERFORMING ORGANIZATION NAME(S) AND ADDRESS(ES) UES Inc. 4401 Dayton-Xenia Rd. Dayton, OH 45432-1894					8. PERFORMING ORGANIZATION REPORT NUMBER 	
9. SPONSORING/MONITORING AGENCY NAME(S) AND ADDRESS(ES) Air Force Research Laboratory Materials and Manufacturing Directorate Wright-Patterson Air Force Base, OH 45433-7750 Air Force Materiel Command United States Air Force					10. SPONSORING/MONITORING AGENCY ACRONYM(S) AFRL/RXCCM	
					11. SPONSORING/MONITORING AGENCY REPORT NUMBER(S) AFRL-RX-WP-TR-2016-0013	
12. DISTRIBUTION/AVAILABILITY STATEMENT Distribution Statement A. Approved for public release; distribution unlimited.						
13. SUPPLEMENTARY NOTES PA Case Number: 88ABW-2015-6174; Clearance Date: 22 Dec 2015. This report contains color.						
14. ABSTRACT (Maximum 200 words) This final report details progress made on various topics related to advanced metallic and advanced metallic composites. In this program, the work covered the material needs for enabling a variety of missions including access to space and hypersonic flight for global access and meeting the continuing demand for higher performance, more efficient jet engines. The focus areas covered a broad range of technologies comprising thermal protection materials, fiber lasers for directed energy, Integrated Computational Materials Science and Engineering (ICMSE), superalloy development, hybrid disks, hot structures for hypersonics, functional materials for energy needs, and nanoenergetic materials for munitions needs. This report will cover three categories of research: advanced ceramics/composites, advanced metals, and functional metals. Much of this research has been published elsewhere in the open literature as journal articles and papers, and is referenced in the text.						
15. SUBJECT TERMS high entropy alloys, titanium, inertia welding						
16. SECURITY CLASSIFICATION OF:			17. LIMITATION OF ABSTRACT: SAR	18. NUMBER OF PAGES 17	19a. NAME OF RESPONSIBLE PERSON (Monitor) Patrick Carlin	
a. REPORT Unclassified	b. ABSTRACT Unclassified	c. THIS PAGE Unclassified			19b. TELEPHONE NUMBER (Include Area Code) 937-904-5547	

Table of Contents

Table of Contents	1
List of Figures	ii
Forward	iii
1.0 Executive Summary	1
2.0 Task Order 0005 – Advanced Metals Research.....	2
2.1 Tension Properties of IFW Joints of Dissimilar Ni-based Superalloys	2
2.2 Cold Rolling of a Refractory High-entropy Alloy	3
2.3 Characterization and Mechanical Behavior of Advanced Aerospace Alloys	4
References	10
List of Acronyms	11

List of Figures

Figure 1: (a) Fracture surface of a LSHR/Mar-M247 weld specimen fractured in Mar-M247 region ~6 mm apart from the weld interface. (b-c) Higher magnification images illustrating (b) a blocky, faceted appearance of fracture and (c) shallow dimples on the faceted surfaces.	2
Figure 2: (a) Fracture surface of a LSHR/Mar-M247 weld specimen fractured at the weld interface illustrating a circular welding defect. (b, c) Higher magnification images illustrating (b) fine carbide and oxide particles inside the welding defect (top) and transition to ductile fracture of the Mar-M247 alloy (bottom), (c) facets and dimples outside the welding defect.	3
Figure 3: OIM maps showing crystallographic orientation spread in the two specimens. (a) Microspecimen A, and (b) Microspecimen B.....	5
Figure 4: Localized deformation in Microspecimen A at the peak stress of 877 MPa. Slip lines corresponding to basal [a] slip in primary α grain and prism [a] slip in transformed β region are marked in (a) and (b), respectively.	5
Figure 5: Localized deformation in Microspecimen B at the peak stress of 830 MPa. Slip lines corresponding to basal [a] slip in primary α grain and prism [a] slip in transformed β region are marked in (a) and (b), respectively.	5
Figure 6: Strain distribution from DIC analysis in gage section of microspecimen A. (a) At the peak stress of 877 MPa, and (b) in the unloaded condition.....	6
Figure 7: Strain distribution from DIC analysis in gage section of microspecimen B. (a) At the peak stress of 830 MPa, and (b) in the unloaded condition.....	6
Figure 8: (a) EBSD pattern from the single crystal specimen. (b) Indexing of the pattern shown in (a) with automatic (i.e. Hough transform based) detection of Kikuchi bands.	8

Forward

This report was prepared by the Materials and Processes Division of UES, Inc., Dayton, Ohio under Air Force Contract No. FA8650-10-D-5226. Mr. Patrick Carlin and Lt. Andrew Nauss of the Structural Materials Division of the Air Force Research Laboratory were the Government Project Engineers. The research reported herein covers the period 16 September 2014 through 21 September 2015.

1.0 Executive Summary

The materials research and development program for the Air Force is largely driven by the perceived needs of high level initiatives such as Versatile Affordable Advanced Turbine Engine (VAATE), Integrated High Performance Rocket Propulsion Technology (IHDRPT), Adaptive Versatile Engine Technology (ADVENT), Integrated Vehicle Energy Technology (INVENT), X-51 Scramjet Engine Demonstrator, and Highly Efficient Embedded Turbine Engine (HEETE). Factors such as the material temperature, design stress, thermal stability, distortion tolerance, expected design life, and environmental resistance requirements vary significantly between these initiatives, between requirements of the eventual weapon systems, and between various components within them. The limiting/enabling properties also vary significantly. Thus there is a need to invest in Research and Development (R&D) on a variety of materials with a breadth sufficient to facilitate eventual optimization of specific property sets that are application specific. Since funding limitations restrict the exploration space, and since there is a need to accelerate the development and transition of advanced materials in a timely manner, computational materials science and engineering is essential.

In this program, the work covered the material needs for enabling a variety of missions including access to space and hypersonic flight for global access and meeting the continuing demand for higher performance, more efficient jet engines. The focus areas covered a broad range of technologies comprising ceramic composites, thermal protection materials, fiber lasers for directed energy, Integrated Computational Materials Science and Engineering (ICMSE), superalloy development, hybrid disks, hot structures for hypersonics, functional materials for energy needs, and nanoenergetic materials for munitions needs. This report will cover two categories of research, advanced metals and functional metals.

2.0 Task Order 0005 – Advanced Metals Research

The work presented in this report was initiated under FA8650-10-D-5226 Task Order 0003 and continued under Task Order 0005.

2.1 Tension Properties of IFW Joints of Dissimilar Ni-based Superalloys

This task is continuation of the solid state joining work described in the FA8650-10-D-5224 Task Order 3 final report. Microstructure, tensile properties, and fracture behavior of the inertia friction weld (IFW) joints of dissimilar superalloys, cast Mar-M247 and wrought low solvus high refractory (LSHR) alloy, were studied to assess the weld quality [1]. Tensile tests were conducted at 23 and 704°C on the samples containing different areas of the weld interface of the same welded material. The stress-strain curves were registered at different axial distances from the weld interface. In all tested samples, plastic deformation was localized on the Mar-M247 side, outside the heat-affected zone (HAZ); inside HAZ, the resistance to plastic deformation of Mar-M247 increased with a decrease in the distance from the weld interface. Only elastic deformation occurred on the LSHR side. Fracture occurred on the Mar-M247 side, outside HAZ (Figure 1), or at the weld interface (Figure 2). In the latter case, welding defects in the form of clusters of nanometer-sized oxide and carbide particles were observed at the fracture surfaces. These results revealed that the IFW process is capable of producing weld joints between Mar-M247 and LSHR with fracture strengths higher than that of Mar-M247. However, optimization of the IFW processing parameters is required to minimize clustering of oxide/carbide particles at the weld interface in this alloy pair.

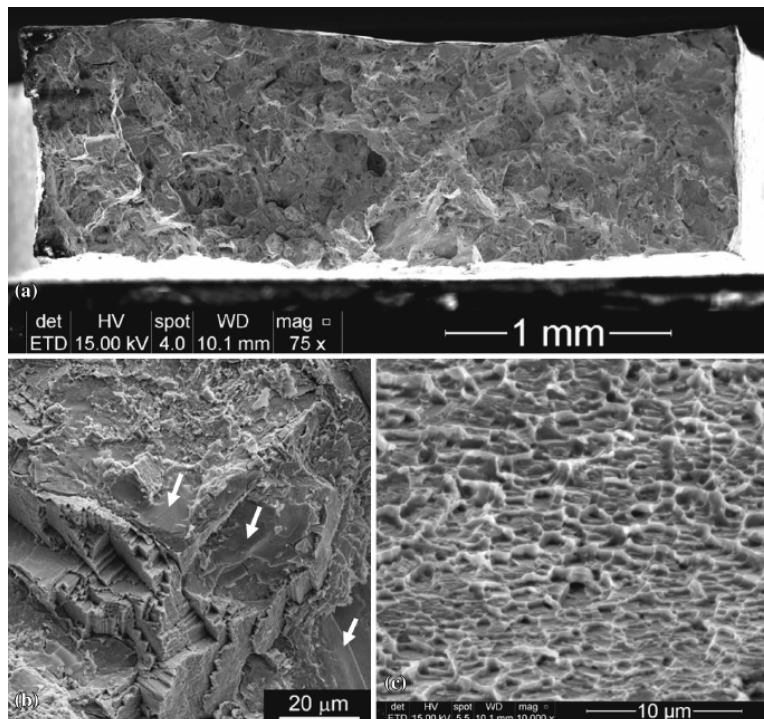


Figure 1: (a) Fracture surface of a LSHR/Mar-M247 weld specimen fractured in Mar-M247 region ~6 mm apart from the weld interface. (b-c) Higher magnification images illustrating (b) a blocky, faceted appearance of fracture and (c) shallow dimples on the faceted surfaces.

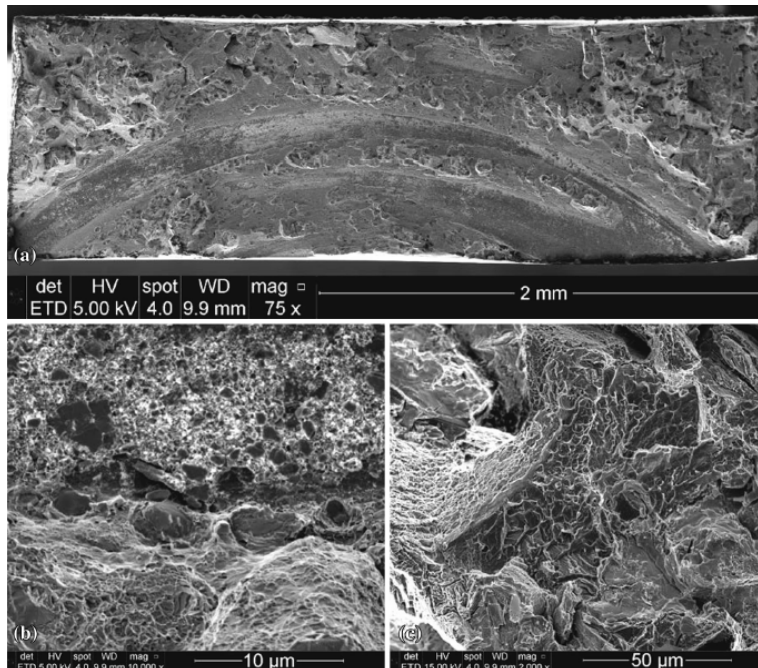


Figure 2: (a) Fracture surface of a LSHR/Mar-M247 weld specimen fractured at the weld interface illustrating a circular welding defect. (b, c) Higher magnification images illustrating (b) fine carbide and oxide particles inside the welding defect (top) and transition to ductile fracture of the Mar-M247 alloy (bottom), (c) facets and dimples outside the welding defect.

2.2 Cold Rolling of a Refractory High-entropy Alloy

We have recently developed a refractory HfNbTaTiZr alloy that exhibits homogeneous plastic flow and marked strain hardening during compression plastic flow at room temperature [2]. Homogeneous plastic flow and excellent ductility during room-temperature compression have been rationalized on the basis of strain hardening originating from solid-solution strengthening and extensive deformation twinning. In the present work, the excellent ductility of HfNbTaTiZr in compression has been utilized to produce thin sheet by cold rolling. The deformation behavior during cold rolling as well as the microstructure and mechanical properties of the rolled sheet in the as-deformed and rolled-and-annealed conditions have been studied. The alloy was successfully rolled at room temperature up to 86.4% reduction in thickness (true thickness strain is 2.3). This represents the first successful attempt to cold roll a high-entropy alloy (HEA) with a body-centered cubic (BCC) crystal structure. The microstructure and properties of the rolled sheets were determined in the as-rolled condition and after annealing at 800 °C, 1000 °C, and 1200 °C. Cold rolling resulted in extensive grain elongation, formation of deformation bands within the grains, and development of crystallographic textures that depended on the rolling reduction. The 86.4% cold-rolled sheet had true tensile stress of 1295 MPa and tensile ductility of 4.7%. After annealing at 1000 °C and 1200 °C, complete recrystallization of the cold-rolled sheet occurred. After annealing at 1000 °C, the true tensile stress and ductility of the sheet were 1262 MPa and 9.7%, respectively.

2.3 Characterization and Mechanical Behavior of Advanced Aerospace Alloys

Micro-Scale Deformation in Polycrystalline Ti-6242

Fatigue crack initiation is a local phenomenon, which can result from site-specific deformation and/or fracture in engineering materials. In titanium alloys, inhomogeneous strain distribution during service arising from anisotropic elasticity and plasticity is known to be a major cause of fatigue crack initiation. To better understand fatigue crack initiation and to better model fatigue indicator parameters (FIPs), an improved understanding of local deformation mechanisms is needed.

Crystal plasticity-based finite element models (CPFEM) have been developed to predict stress and strain redistributions under applied loads in engineering alloys, including titanium alloys. Constitutive behavior of titanium single crystal and single colony specimens are important inputs in these models. Validation of CPFEM predictions with experimental results on millimeter-scale samples remains a challenge, as in-situ experimental observations and measurements of deformation in a large number (≥ 100) of grains is difficult. High energy diffraction microscopy (HEDM) techniques are proving useful in interrogating large-volume specimens. However, only the elastic part of total strain is measured directly with HEDM. The micrometer-scale specimens have limited number of grains (typically < 100) and the deformation in a larger fraction of total specimen volume can be monitored in-situ. Therefore, the micro-scale specimens provide a better means to validate the CPFEM predictions than the millimeter-scale samples.

In the current study, micro-scale specimens of Ti-6Al-2Sn-4Zr-2Mo were prepared via focused ion beam (FIB) methods [3]. The in-situ tension tests were run in a scanning electron microscope (SEM), and strain was quantified using digital image correlation (DIC) techniques. The micromechanisms of localized deformation were elucidated via high resolution images acquired during the test and analyses of electron backscattered diffraction (EBSD) data.

The EBSD data were collected for the two specimens and orientation imaging microscopy (OIM) maps were plotted based on the inverse pole figure (IPF) as well as the Schmid factors for basal and prism slips (Figure 3). In-situ tension tests were run in an SEM and the high resolution images were analyzed with DIC to determine the strain evolution during the test. The high resolution images were also used to identify the evidence of localized slip (Figure 4 and Figure 5). The localized slip in both the primary α grains and transformed β regions in the two specimens could be understood on the basis of Schmid factor analyses. The strain distributions determined with DIC (Figure 6 and Figure 7) are consistent with the observations of localized slip in the two specimens.

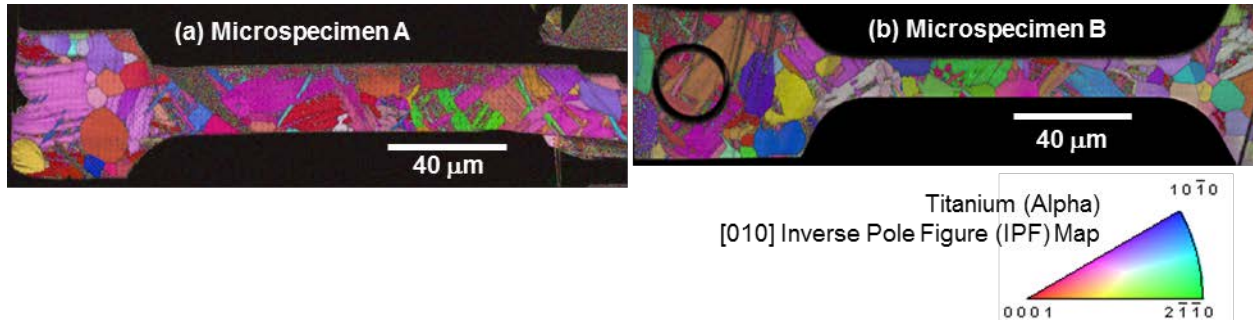


Figure 3: OIM maps showing crystallographic orientation spread in the two specimens. (a) Microspecimen A, and (b) Microspecimen B.

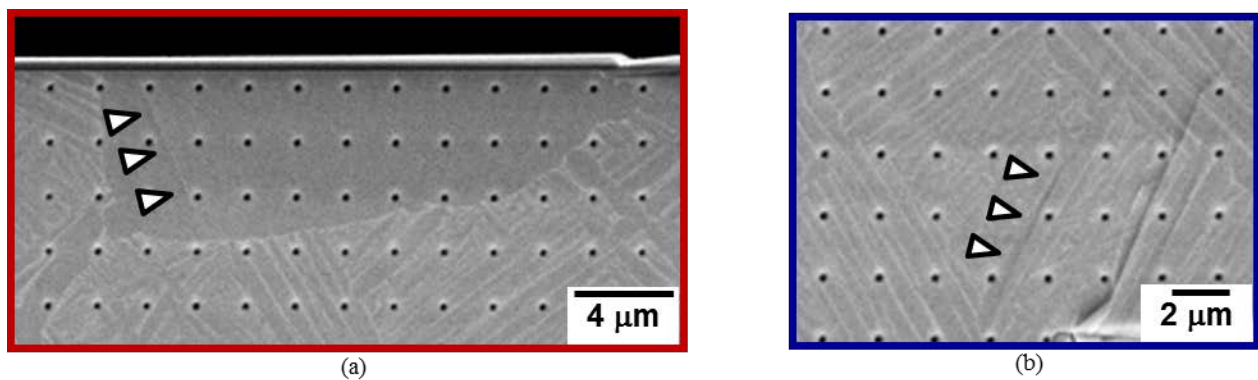


Figure 4: Localized deformation in Microspecimen A at the peak stress of 877 MPa. Slip lines corresponding to basal $[a]$ slip in primary α grain and prism $[a]$ slip in transformed β region are marked in (a) and (b), respectively.

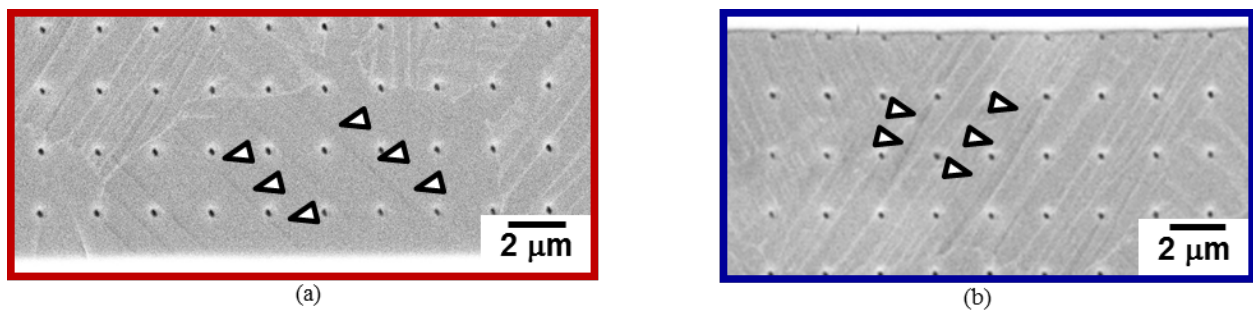


Figure 5: Localized deformation in Microspecimen B at the peak stress of 830 MPa. Slip lines corresponding to basal $[a]$ slip in primary α grain and prism $[a]$ slip in transformed β region are marked in (a) and (b), respectively.

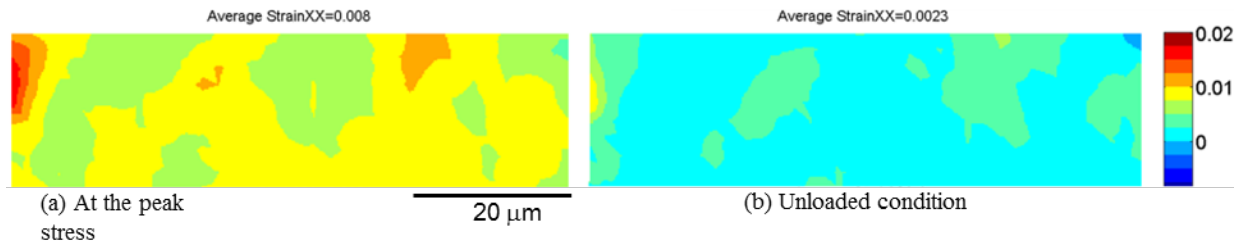


Figure 6: Strain distribution from DIC analysis in gage section of Microspecimen A. (a) At the peak stress of 877 MPa, and (b) in the unloaded condition.

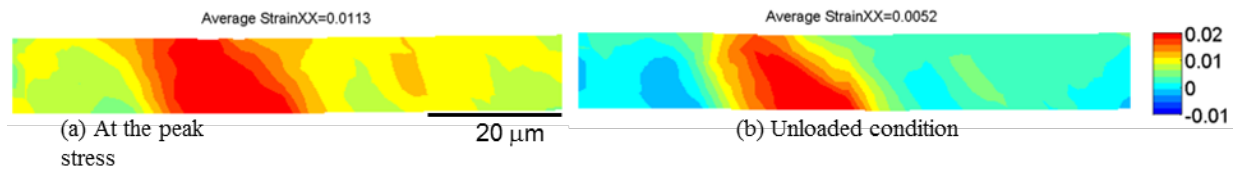


Figure 7: Strain distribution from DIC analysis in gage section of Microspecimen B. (a) At the peak stress of 830 MPa, and (b) in the unloaded condition.

Life-Limiting Fatigue Failures in Titanium Alloys

Fatigue life prediction of fracture critical parts is often dictated by the minimum rather than the mean fatigue behavior. In order to obtain the minimum lifetime limit, a statistical distribution is often fit to the fatigue data, which is extrapolated to the desired probability level, *e.g.* the 1 in 1000 probability of failure or the B0.1 lifetime, to determine the minimum lifetime. Fatigue lifetime data tends to capture the mean fatigue behavior quite well, for example, a stress vs. lifetime or the S-N plot provides a good depiction of the mean lifetime trend and, depending on the number of tests at each stress level, also gives a sense for the distribution about the mean. The distribution with respect to the mean behavior, however, may not extrapolate to the realistic minimum lifetime limit. This is because the mean and the minimum behaviors are controlled by different mechanisms and respond at different rates to changes in stress level, microstructure, and other variables. Furthermore, while the mean lifetime has increasing contribution from the crack-initiation lifetime as the stress level is decreased, the minimum lifetime is found to be largely controlled by small and long crack growth lifetime. Since crack-initiation lifetime is often more sensitive to stress level and other variables than the crack growth regime, this produces a separation between the mean and the minimum behavior as the stress level is decreased.

In this study, the minimum lifetime mechanism or the minimum lifetime failure is referred to as the life-limiting mechanism or the life-limiting failure [4]. In addition to an accurate assessment of the minimum lifetime limit, it is also important to estimate the probability of occurrence of the life-limiting mechanism. As mentioned before, the life-limiting failures often occur by a different mechanism than the mean-lifetime failure but also tend to initiate from a rarer combination of microstructural phases. As a result, the probability of occurrence of such failures will decrease with decreasing stress level and it may require an increasingly large number of tests to characterize the life-limiting failures in lab-scale specimen volumes. The probability of the life-limiting failures will however increase with volume and can be significant on the scale of a

fracture-critical component. The main goal of this work is to shed light on the life-limiting mechanism in Ti-6Al-2Sn-4Zr-2Mo (Ti-6-2-4-2) with respect to other titanium alloys and develop an understanding of the probability of occurrence of life-limiting failures with respect to stress level and specimen volume. A modeling approach for microstructure-based prediction of the probability of life-limiting failures in titanium alloys is presented for a single phase α -titanium microstructure using contiguous slip length as the fatigue deformation metric. The results are discussed with respect to experimental trends.

The following main conclusions can be drawn from this study: (i) The life-limiting crack initiation mechanism in Ti-6-2-4-2 was similar to that found in other $\alpha+\beta$ titanium alloys including Ti-6-2-4-6 and Ti-6-4. (ii) A microstructure-based model of the distribution in lifetimes of the life-limiting failures, using the distribution in α_p sizes, an assumption for the small-crack growth threshold, and the small crack growth data as inputs, was shown to reasonably predict the experiment. (iii) A model for microstructure-based prediction of the probability of occurrence of life-limiting failures was illustrated using a single-phase α -Ti microstructure in which the slip band crack initiation mechanism due to configurations of grains with contiguous slip path was invoked. The results exhibited trends similar to that seen experimentally in titanium alloys.

Characterization of Facet Crystallography with Electron Backscattered Diffraction

Automated EBSD techniques have recently been used successfully and extensively for detailed microstructural quantifications, including 3-dimensional characterization. For typical EBSD characterizations, sample preparation methodology is optimized to obtain patterns of good quality. For direct characterization of fracture features, such as facets, the option of surface optimization is not available. Furthermore, the fracture facets are typically not perpendicular to the electron beam direction in an SEM at the stage tilt of 0° , as is the case for specimens prepared specifically for EBSD characterization. This poses unique challenges for characterization of fracture facets with EBSD.

In a typical OIM characterization using EBSD, the SEM stage is tilted to 70° and the background is collected from a flat polished surface of a specimen, while the electron beam is in the fast-scan mode. The OIM system is usually calibrated for this tilt of 70° . After background collection, the electron beam is switched from scan mode to spot mode to obtain EBSD patterns from the flat sample in the same spatial orientation at which the background had been collected (Figure 8). However, if the sample is inclined with respect to this orientation, an intensity gradient is seen in the EBSD pattern after background correction. Field reported that the intensity gradient becomes very strong, even at low inclinations away from the initial orientation used for background collection. It is further reported that at the angular difference between the orientations for background and diffraction pattern collection (ϕ) = 5° , this intensity gradient becomes so severe that any EBSD pattern would be occluded [5]. On the other hand, Sinha *et al.* have reported fracture facet crystallography results obtained using EBSD at ϕ as high as 18° [6] and 24° [7]. Furthermore, Davies and Randle [8] have reported crystallographic orientations determined via EBSD for ϕ up to $\pm 30^\circ$.

Although the OIM images of facets (typically obtained via automated scans of characterized regions) were not provided in references [6-9] and the crystallography was determined based on the EBSD patterns from discrete locations on the facets, the information was useful in determining the fracture mechanisms. For example, it was demonstrated that the crystallography of facets changed with the type of loading in Ti-alloys [6, 7], and the dominant cleavage planes in steels were $\{001\}$ [8, 9]. In view of the apparent disagreement on the limitation on ϕ , an improved clarification on strengths and limitations of EBSD for fracture facet characterization is needed.

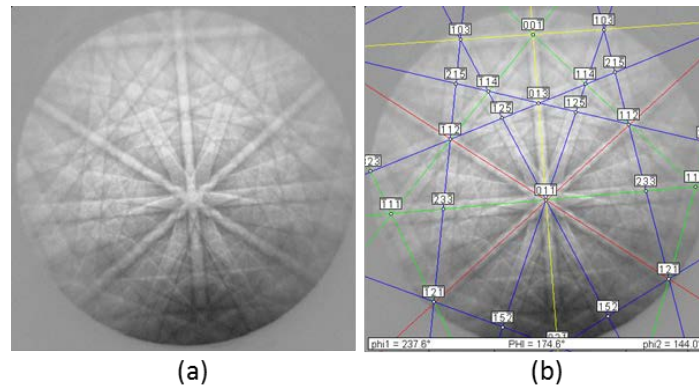


Figure 8: (a) EBSD pattern from the single crystal specimen. (b) Indexing of the pattern shown in (a) with automatic (i.e. Hough transform based) detection of Kikuchi bands.

In the current study, the background was collected from the polished flat surface of a polycrystalline Ni-base superalloy, IN100 [10]. The EBSD patterns were collected from the polished surface of a single crystal Ni-base superalloy at angles ranging between 0 and 50° from the orientation for background collection (i.e. $\phi = 0$ to 50°). The two limiting orientations of the normal to surface for pattern collection are considered: (i) This normal lies in the plane formed by electron beam direction and tilt axis (at the SEM stage tilt of 0°), and (ii) it lies in the plane perpendicular to the tilt axis. For each orientation, the feasibility of acquiring indexable EBSD patterns was assessed. The results are discussed in the context of applicability of this method for characterization of crystallography of fracture facets and fracture mechanisms associated with facet formation. Though the experiments are carried out on a Ni-base superalloy, the results are expected to be equally relevant for other crystalline materials, including Ti-alloys, Al-alloys and steels. Moreover, the methodology can be applied for crystallographic characterization of facets formed not only from fracture but also by any other mechanisms (e.g. growth facets).

In the current study, polished surfaces of single crystal Ni-base superalloy, with their normals inclined with respect to the electron beam direction at angles $\alpha = 0 - 50^\circ$ (at the SEM stage tilt of 0°), were characterized via EBSD. The results indicate that at $\alpha > 0^\circ$, only a partial EBSD pattern is obtained, when the background is collected from a polycrystalline specimen with spatial orientation corresponding to $\alpha = 0^\circ$. The farther the angle α is away from 0°, the smaller the fraction of full EBSD pattern obtained.

Prior studies have reported that only the facets with $\alpha \leq 5^\circ$ are amenable to characterization with EBSD. However, the results of the current study indicate that facets with $\alpha \leq 50^\circ$ can be

characterized with EBSD. For $\alpha \leq 50^\circ$, the fraction of obtained pattern is large enough to be indexed automatically with TSL OIM Data Collection software (EDAX, Inc.), when the surface normal lies (at the SEM stage tilt of 0° , prior to tilting to 70° for EBSD pattern collection) in the plane formed by electron beam direction and SEM stage tilt axis. However, when the surface normal lies in the plane perpendicular to the tilt axis, the fraction of EBSD pattern for $\alpha = 30^\circ$ is too small to be indexed automatically. Nevertheless, correct indexing was possible by first *manually* detecting the Kikuchi bands in the partial EBSD pattern. For this orientation of surface normal with respect to the tilt axis, the fraction of EBSD pattern for $\alpha = 50^\circ$ is smaller than for $\alpha = 30^\circ$ and it cannot be indexed in this particular case.

The results of the current study also show that non-zero values of α have no influence on the IPFs for Z and Y-axes, as the crystallographic orientation of the analyzed surface remains fixed. Therefore, the inclination angle (α) of characterized surface (*e.g.* facet) does not need to be taken into account during analysis of data (*e.g.* using TSL OIM Analysis software, EDAX, Inc.) to depict its crystallographic orientation. However, to show the position of the surface (facet) normal on the IPF, one must account for the spatial orientation of characterized facet.

This study has significant implications for quantitative characterization of fracture facets, as these features are rarely oriented with their normals aligned with the electron-beam direction (*i.e.* $\alpha = 0^\circ$) at the SEM stage tilt of 0° , prior to tilting to 70° for EBSD pattern collection. Moreover, the angle α varies from one facet to another on the same fracture surface. Prior studies have reported that only the inclinations with $\alpha \leq 5^\circ$ are amenable to characterization by direct EBSD on facets. However, the current study establishes that this range of α for successful characterization with direct EBSD can be extended from $0 - 5^\circ$ to $0 - 50^\circ$, if one were to take advantage of the SEM stage rotations. It may not be possible to obtain the complete orientation image of the facets with α significantly higher than the optimum 0° . However, the quantitative crystallographic orientation determined at a few discrete points on a particular facet can provide important and sufficient information on the associated fracture mechanisms.

Although the results of the current study are discussed in the context of characterization of fracture facets, their implications are more general and this methodology is equally relevant for characterization of other kinds of facets, including growth facets.

References

- [1] O.N. Senkov, D.W. Mahaffey, S.L. Semiatin, and C. Woodward, "Site-Dependent Tension Properties of Inertia Friction-Welded Joints Made From Dissimilar Ni-based Superalloys," *Journal of Materials Engineering and Performance*, vol. 24, pp. 1173-84 (2015).
- [2] O.N. Senkov and S.L. Semiatin, "Microstructure and properties of a refractory high-entropy alloy after cold working," *Journal of Alloys and Compounds*, vol. 649, pp. 1110-1123 (2015).
- [3] V. Sinha, S.K. Jha, R. Wheeler, A.L. Pilchak, R. John, and J.M. Larsen, "Deformation Mechanisms in Micro-Scale Specimens of Polycrystalline Ti-6242," *Ti-2015: Proceedings of the 13th World Conference on Titanium (in Press)*.
- [4] Sushant Jha, Adam Pilchak, Christopher Szczepanski, Vikas Sinha, Reji John, and James Larsen, "Probability of Life-Limiting Fatigue Failures in Titanium Alloys," *Ti-2015: Proceedings of the 13th World Conference on Titanium (in Press)*.
- [5] D.P. Field, "Recent advances in the application of orientation imaging," *Ultramicroscopy*, vol. 67, pp. 1-9 (1997).
- [6] V. Sinha, M.J. Mills, and J.C. Williams, "Determination of crystallographic orientation of dwell-fatigue fracture facets in Ti-6242 alloy," *Journal of Materials Science*, vol. 42, no. 19, pp. 8334-8341 (2007).
- [7] V. Sinha, M.J. Mills, and J.C. Williams, "Crystallography of fracture facets in a near-alpha titanium alloy," *Metallurgical and Materials Transactions A*, vol. 37A, pp. 2015-2026 (2006).
- [8] P.A. Davies and V. Randle, "Combined application of electron backscatter diffraction and stereo-photogrammetry in fractography studies," *Journal of Microscopy*, vol. 204, Part 1, pp. 29-38 (2001).
- [9] P.A. Davies, M. Novovic, V. Randle, and P. Bowen, "Application of electron backscatter diffraction (EBSD) to fracture studies of ferritic steels," *Journal of Microscopy*, vol. 205, no. 3 pp. 278 (2002).
- [10] V. Sinha and J.M. Larsen, "Effects of Spatial Orientation of Analyzed Surfaces on Electron Backscattered Diffraction Patterns and Implications for Characterization of Facet Crystallography," *Journal of Materials Science*, (Submitted).

List of Acronyms

Acronym/ Abbreviation	Description
ADVENT	Adaptive Versatile Engine Technology
AFRL	Air Force Research Laboratory
BCC	Body-Centered Cubic
CPFEM	Crystal plasticity-based finite element models
DIC	Digital Image Correlation
EBSA	Electron Back Scattered Diffraction
FEM	Finite-Element Method
FIB	Focused Ion Beam
FIP	Fatigue Indicator Parameters
HAZ	Heat Affected Zone
HEA	High-Entropy Alloys
HEDM	High Energy Diffraction Microscopy
HEETE	Highly Efficient Embedded Turbine Engine
ICMSE	Integrated Computational Materials Science and Engineering
IFW	Inertia Friction Welding
IHPRT	Integrated High Performance Rocket Propulsion Technology
INVENT	Integrated Vehicle Energy Technology
IPF	Inverse Pole Figure
LSHR	Low Solvus High Refractory
OIM	Orientation Imaging Microscopy
R&D	Research and Development
SEM	Scanning Electron Microscope
VAATE	Versatile Affordable Advanced Turbine Engine